A model for evaluating continental chemical weathering from riverine transports of dissolved major elements at a global scale

Juan-Luis Lechuga-Crespo, J.M. Sánchez-Pérez, Sabine Simeoni-Sauvage, Jens Hartmann, Philippe Amiotte-Suchet, Jean-Luc Probst, Estilita Ruiz-Romera

A model for evaluating continental chemical weathering from riverine transports of dissolved major elements at a global scale

J.L. Lechuga-Crespo[a,b,**], J.M. Sánchez-Pérez[a,*], S. Sauvage[a], J. Hartmann[c], P. Amiotte Suchet[d], J.L. Probst[a], E. Ruiz-Romera[b]

[a] Laboratoire Ecologie fonctionnelle et Environnement, Université de Toulouse, CNRS, INPT, UPS, Campus ENSAT, Avenue de l'Agrobiopole, 31326 Castanet Tolosan, CEDEX, France
[b] Department of Chemical and Environmental Engineering, University of the Basque Country, Plaza Ingeniero Torres Quevedo 1, Bilbao 48013, Basque Country, Spain
[c] Institut for Geology, Department of Geosciences, Center for Earth System Research and Sustainability (CEN), Universität Hamburg, Bundesstraße 55, 20146 Hamburg, Germany
[d] Biogéosciences, UMR 6282, CNRS, University of Bourgogne Franche-Comté, 6 boulevard Gabriel, Dijon F-21000, France

ARTICLE INFO

Keywords:
Empirical model
Ionic flux
Chemical weathering
Global scale

ABSTRACT

This study presents a process-based-empirical model for the assessment of ionic fluxes derived from chemical weathering of rocks (ICWR) at a global scale. The equations are designed and the parameters fitted using riverine transport of dissolved major ions Ca^{2+}, Mg^{2+}, K^{+}, Na^{+}, Cl^{-}, SO_4^{2-}, and alkalinity at a global scale by combining point sampling analysis with spatial descriptions of hydrology, climate, topography, lithology and soil variables such as mineral composition and regolith thickness. Different configurations of the model are considered and the results show that the previously reported "soil shielding" effect on chemical weathering (CW) of rocks presents different values for each of the ions considered. Overall, there is good agreement between median and ranges in observed and simulated data, but further analysis is required to downscale the model to catchment scale. Application to the global scale provides the first global ICWR map, resulting in an average cationic flux derived from chemical weathering of $734{\cdot}10^6$ Mg·y^{-1}, where 58% is Ca^{2+}, 15% is Mg^{2+}, 24% is Na^{+} and 3% is K^{+}, and an average anionic flux derived from chemical weathering of $2640{\cdot}10^6$ Mg·y^{-1}, where 74% is alkalinity, 18% is SO_4^{2-}, and 8% is Cl^{-}. Hyperactive and hotspot areas are elucidated and compared between ions.

1. Introduction

Freshwater chemical composition has long been used as a proxy to understand the processes occurring in a catchment (e.g. Gibbs, 1970; Amiotte Suchet and Probst, 1993a; Romero-Mujalli et al., 2019). The insights obtained from these analyses are relevant for assessing biogeochemical cycles, since rivers are vectors of matter transport between land and oceans (Probst, 1992). Major ion riverine loads are linked to the mineralogical composition of the underlying bedrock and overlying soil, and to their sensitivity to chemical weathering (CW) (Hartmann et al., 2009). CW of rocks is the process responsible for transforming rock into saprolites and soils, i.e. soil pedogenesis, in the Critical Zone (CZ) (Riebe et al., 2017), which releases dissolved compounds that are subsequently transported by rivers.

For several decades, evaluation and quantification of CW has been the focus of hydrogeochemical research (Livingstone, 1963; White and Blum, 1995; Di Figlia et al., 2007; Jansen et al., 2010; Hartmann et al., 2014a; Raab et al., 2019) and in more recent years it has also been used to quantify trends in salt increases related to human activities (Meybeck, 2003; Moosdorf et al., 2011; Guo et al., 2015; Kaushal et al., 2018). Large-scale studies have focused CW analysis on its implications for atmosphere/land/ocean fluxes and the Earth's climate, in influencing the biogeochemical cycles of elements by regulating CO_2 consumption, or nutrient release (Amiotte Suchet and Probst, 1993b; Amiotte Suchet and Probst, 1995; Dupré et al., 2003; Hartmann et al., 2014a). However, fewer studies have centred on individual ion analysis (e.g. Goddéris et al., 2006; Goddéris et al., 2009) and, to the authors' knowledge, there is no spatially explicit reference product for ionic

* Corresponding author.
** Corresponding author at: Laboratoire Ecologie fonctionnelle et Environnement, Université de Toulouse, CNRS, INPT, UPS, Campus ENSAT, Avenue de l'Agrobiopole, 31326 Castanet Tolosan, CEDEX, France; Department of Chemical and Environmental Engineering, University of the Basque Country, Plaza Ingeniero Torres Quevedo 1, Bilbao 48013, Basque Country, Spain.
E-mail addresses: juanluis.lechuga@ehu.eus (J.L. Lechuga-Crespo), jose.sanchez@univ-tlse3.fr (J.M. Sánchez-Pérez).

https://doi.org/10.1016/j.gloplacha.2020.103226

fluxes derived from chemical weathering of rocks (ICWR) at a global scale that quantifies the natural rock fluxes of single ions.

Assessment of chemical weathering rates (CWR) at catchment-to-global scale has evolved over recent years due to improvements in laboratory experiments, the compilation of river water chemical databases, and the development of technical resources in modelling (Meybeck, 1987; Amiotte Suchet and Probst, 1993a, 1995; Probst et al., 1994; Hartmann et al., 2014a; Perri et al., 2016; Dong et al., 2018; Biondino et al., 2020). A distinction can be drawn between two main approaches to hydrogeochemical modelling: mechanistic and empirical based models. On the one hand, mechanistic models such as WHAM (Tipping, 1994) or WITCH (Goddéris et al., 2006) base their calculation on distinguishing between several layers in the soil with different chemical weathering rates, integrating the chemical composition of soils and the drainage waters in a mass-balance where the dissolution of primary minerals is described through kinetic laws (Goddéris et al., 2006; Roelandt et al., 2010), though they require a large quantity of detailed data which is normally not available worldwide. On the other hand, empirical models relate CWR to environmental variables through linear and non-linear regression, using statistically fitted parameters (Meybeck, 1987; Amiotte Suchet and Probst, 1995; Dessert et al., 2003; Hartmann, 2009), ignoring the physical dynamics behind the process. Despite their greater degree of abstraction, empirical laws have extensively been used to quantify global fluxes of matter (Hartmann et al., 2014a) and CO_2 sequestration by rock weathering (Amiotte Suchet and Probst, 1995; Probst et al., 1997; Dessert et al., 2003; Hartmann et al., 2009), since they require less exhaustive input data and fewer computing resources while at the same time providing a useful product.

Given that, to the best of the authors' knowledge, there are no spatially explicit results at a global scale for the contribution of each major ion to the total CWR, and that this needs to be quantified before assessing the global anthropogenic inputs of major ions (Vörösmarty et al., 2010),the present study seeks to develop and apply an empirical model at a global scale to quantify the ICWR of major elements. The methodology pursued is based on that presented by Hartmann et al. (2009), and the objectives are: *i)* to present the methodology used to develop a spatially explicit empirical model of ICWR; *ii) to* evaluate the limitations of this methodology and of application of the model; and *iii)* to present and contrast the preliminary results of the model at a global scale, including a discussion of spatial distribution and an assessment of hyperactive and hotspot areas.

2. Materials and methods

2.1. Conceptualization

Conceptualization of the CW process used in developing this model is explained in the following lines and shown in graphic form in the Supplementary Information, Fig. S1. Major ion fluxes — i.e. Ca^{2+}, Mg^{2+}, K^+, Na^+, Cl^-, SO_4^{2-}, and alkalinity (HCO_3^- + CO_3^{2-})— in rivers have previously been used as a proxy of all the processes occurring in the upstream draining catchment (Garrels and Mackenzie, 1972; Meybeck, 1984, 1986; Hartmann and Moosdorf, 2011), and are also considered in the present study. Two sources are established with regards to the spatial unit of the catchment: allochthonous, when the origin of the element lies outside the boundaries of the catchment (i.e. atmospheric dry and wet deposition); and autochthonous when the source of the element lies within the catchment area (i.e. bedrock chemical weathering). Human activity is a third source of ions in rivers, which may be: *allochthonous* when ions originating from anthropogenic activities are brought to the river by atmospheric deposition, e.g. acid rain (Schindler, 1988; Likens et al., 1996; Mahowald et al., 2011); or *autochthonous* when there are spot saline sources or diffuse input within the unit, such as effluents from wastewater treatment plants (Carey and Migliaccio, 2009), cropland fertilization, or road salting (Moore et al., 2008; Dailey et al., 2014). The conceptual schema of the major ion biogeochemical cycle adopted in this study is shown in the Supplementary Information, Fig. S1.

Atmospheric deposition incorporates ions to the CZ (from above the ground through the soil and saprolite horizons to the bedrock, Keller, 2019) which are either concentrated in the soil surface by evapotranspiration and washed out of the catchment through surface and subsurface runoffs; or infiltrated into the saprolite down to the unsaturated and saturated zones, reaching the groundwater reservoir. Soil processes —such as organic matter decay and root uptake followed by biomass storage— interact with these salts and may present synergies with the transport fluxes, altering the concentration of the salts present in the lateral flow (or subsurface runoff) and subsequently the river water (Keller, 2019). As regards the groundwater source, salts are derived from water interaction with rocks and later transported to the stream with groundwater flow (or baseflow).

CW has long been reported as a dominant process in major water composition, and several studies (Garrels and Mackenzie, 1972; Stallard and Edmond, 1981; Velbel, 1993; Gaillardet et al., 1999; Balagizi et al., 2015) have highlighted the relevance of lithology, hydrology, soil chemistry, and temperature, as variables that condition both CW and soil processes, while distance to the coast and altitude mostly affect atmospheric deposition (Meybeck et al., 1986, Vet et al., 2014). The combination of all these variables, in addition to human input, condition major ion loads leaving the catchment.

Other dissolved compounds may be found in the dissolved riverine loadings which may interact with major ions, such as SiO_2, NO_3^-, or PO_4^{3-}. However, these elements have not been included within the scope of the modelling, since their global biogeochemical cycles are more complex and more closely linked to biological interactions (c.f. Galloway et al., 2004, Hartmann et al., 2014a) than those of the major ions selected, which are assumed to have more similar pathways between reservoirs and a more stable temporal evolution (Keller, 2019).

2.2. Workflow and data overview

In order to estimate the specific fluxes of major ions, i.e. Ca^{2+}, Mg^{2+}, K^+, Na^+, Cl^-, SO_4^{2-}, and alkalinity, linear regressions have been developed using global databases as input data, fitting the parameters of the equations to minimize the difference between modelled and observed data. The mathematical approach used to develop the equations and fit the parameters is based on previous literature (e.g. Meybeck, 1979; Amiotte Suchet and Probst, 1993a, 1993b; Hartmann, 2009).

The observed chemical concentrations used in this study were taken from the GLORICH database (Hartmann et al., 2014b, retrieved from https://doi.pangaea.de/10.1594/PANGAEA.902360), which compiles over 1.2 million analyses of river waters around the world, as well as containing additional information on the draining catchments at the sampling locations. In order to focus on sampling locations mainly affected by atmospheric deposition and chemical weathering fluxes, a subset of the samples was created (see Section 2.2.1). The specific chemical fluxes were derived from averaged chemical concentrations and specific discharge for each draining catchment, and the differentiation between the atmospheric and chemical weathering contribution was computed using an independent dataset to estimate the atmospheric deposition (see Section 2.2.2). Additional variables were then included in the analysis, such as soil type abundance taken from the Harmonized World Soil Database (HSWD, FAO et al., 2012), regolith thickness (GSDE, Shangguan et al., 2017), and soil permeability (GLHYMPS, Huscroft et al., 2018). The incorporation of these databases is described in Section 2.2.3 and a summary of the uncertainties may be found in Section 2.2.4. The workflow followed is shown in graphic form in Fig. 1.

2.2.1. Data subset and estimation of atmospheric deposition

The original chemical data stored in the GLORICH HC was sorted to

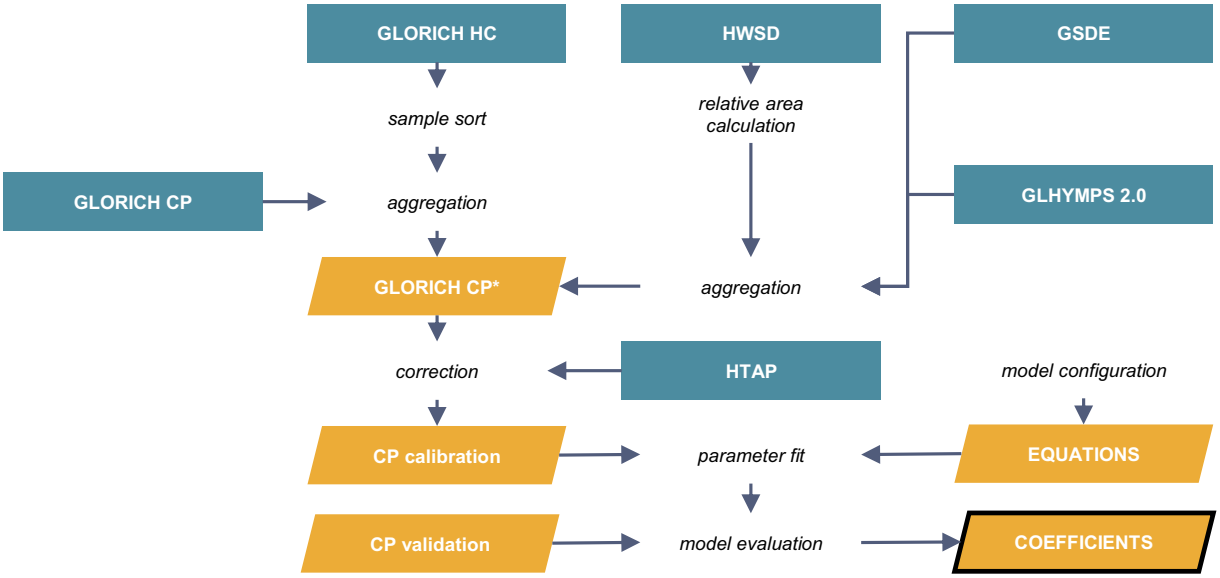

Fig. 1. Workflow summary. The green rectangles represent the original databases included in the analysis, while the yellow boxes contain the datasets derived for the present analysis, and the arrows describe actions. The acronyms refer to: the GLORICH database (Hartmann et al., 2014b) which contains information on hydrochemical analyses (HC) and catchment properties (CP); the Harmonized World Soil Database (HSWD, FAO et al., 2012); the global regolith thickness (GSDE, Shangguan et al., 2017); the soil permeability (GLHYMPS 2.0, Huscroft et al., 2018); and the world precipitation chemistry dataset (HTAP, Vet et al., 2014). (For interpretation of the references to colour in this figure legend, the reader is referred to the web version of this article.)

exclude samples with missing data for Ca^{2+}, Mg^{2+}, K^{+}, Na^{+}, Cl^{-}, SO_4^{2-} or alkalinity, samples showing an ionic charge balance error over ±10% and sampling locations with <3 samples. Around 65% of the original 1,274,102 samples analysed in 18,897 locations between 1942 and 2011 were excluded. Chemical concentrations at the sampling location were aggregated through the median value since the distribution was non-normal according to a Shapiro-Wilk test ($p < 0.01$). Not all sampling locations presented an associated draining catchment, and some were nested catchments; these were also excluded, resulting in 1751 catchments ranging from 1 to $2.9{\cdot}10^4$ km^2, with 3 to 1220 samples, depending on the catchment. A map showing the selected sampling locations and associated areas may be seen in Fig. 2.

2.2.2. Estimation of derived variables and atmospheric deposition

Due to the heterogeneity of the data on the number of samples in each sampling location and the frequent lack of instantaneous discharge, average riverine specific fluxes, F_x measured in $mol{\cdot}m^{-2}{\cdot}y^{-1}$, were estimated from riverine concentration and specific runoff (computed as the discharge at the outlet of the catchment divided by the draining area, Fekete et al., 2002) using Eq. 1. In this equation, specific runoff, q_{ann}, measured in $mm{\cdot}y^{-1}$, was multiplied by the average concentration C_x of the sampling location, measured in $mol{\cdot}L^{-1}$, for each ion x.

$$F_x = q_{ann}{\cdot}C_x \quad (1)$$

Riverine-specific fluxes include the mass departing the catchment from bedrock weathering, atmospheric deposits and other sources (including anthropogenic activities). In order to estimate ICWR, it was necessary to subtract the contribution of atmospheric deposition (Meybeck, 1983). Anthropogenic input could not be quantified since the extent of the anthropic influence differs between catchments; it was therefore assumed to be negligible for major cations and anions at the scale of application. However, further research on the impact of human pressure is needed (Vörösmarty et al., 2010).

Atmospheric flux was estimated using the results of Vet et al. (2014) (HTAP database) on atmospheric seasalt and sulphur deposition. First, the mean seasalt flux throughout the catchment was computed for each catchment using the "raster" package in R (Hijmans, 2019). In order to distinguish the contribution of each ion in the total salt deposition, an ionic concentration distribution profile was then calculated for coastal and continental zones in each continent. To compute these profiles, the raw data used in Vet et al. (2014), obtained from the World Data Precipitation Chemistry website (http://wdcpc.org/global-assessment-data) was classified by continents and into coastal/continental, based on distance from the coast. Average concentration values and ratios to the total salt concentration were then computed (see chemical distribution profiles in Supplementary Information Fig. S2 and Table S1).

Once the percentages of each element within the total concentration were obtained, the catchments were classified into zones according to the position of their centroid. This classification, together with the mean seasalt deposition flux, allowed us to quantify the specific atmospheric flux for each element in each catchment. CW fluxes were computed by subtracting the atmospheric deposition flux from the riverine flux.

2.2.3. Database integration

Spatial analysis was performed using ArcGIS 10.4 and mainly consisted of summarising raster files in the polygonal shapes of the draining catchment. All data was integrated using R software (R Core Team, 2018). Three worldwide databases were included in the original GLORICH catchment properties (CP) database. For each catchment, the cover percentage of each HSWD soil type (FAO et al., 2012) was computed, and the mean regolith depth (Shangguan et al., 2017) and mean hydraulic conductivity (Huscroft et al., 2018) were then summarised. The spatial resolution is different for each database included; the catchment borders were delimited using the Hydro1K database (c.f. Hartmann et al., 2014b) at a 30 arc-second resolution, the same as for the HWSD soil type database (FAO et al., 2012) and hydraulic conductivity (Huscroft et al., 2018). However, finer resolution is found for the global soil depth database (Shangguan et al., 2017). Uncertainties in dataset collection are discussed in Section 2.2.4. However, considering the global approach of the study and the relatively small size of some catchments (see Supplementary Information, Fig. S2), the spatial resolution of the global databases was considered sufficient to represent the lithological and soil compositions, average soil depth, and hydraulic conductivity.

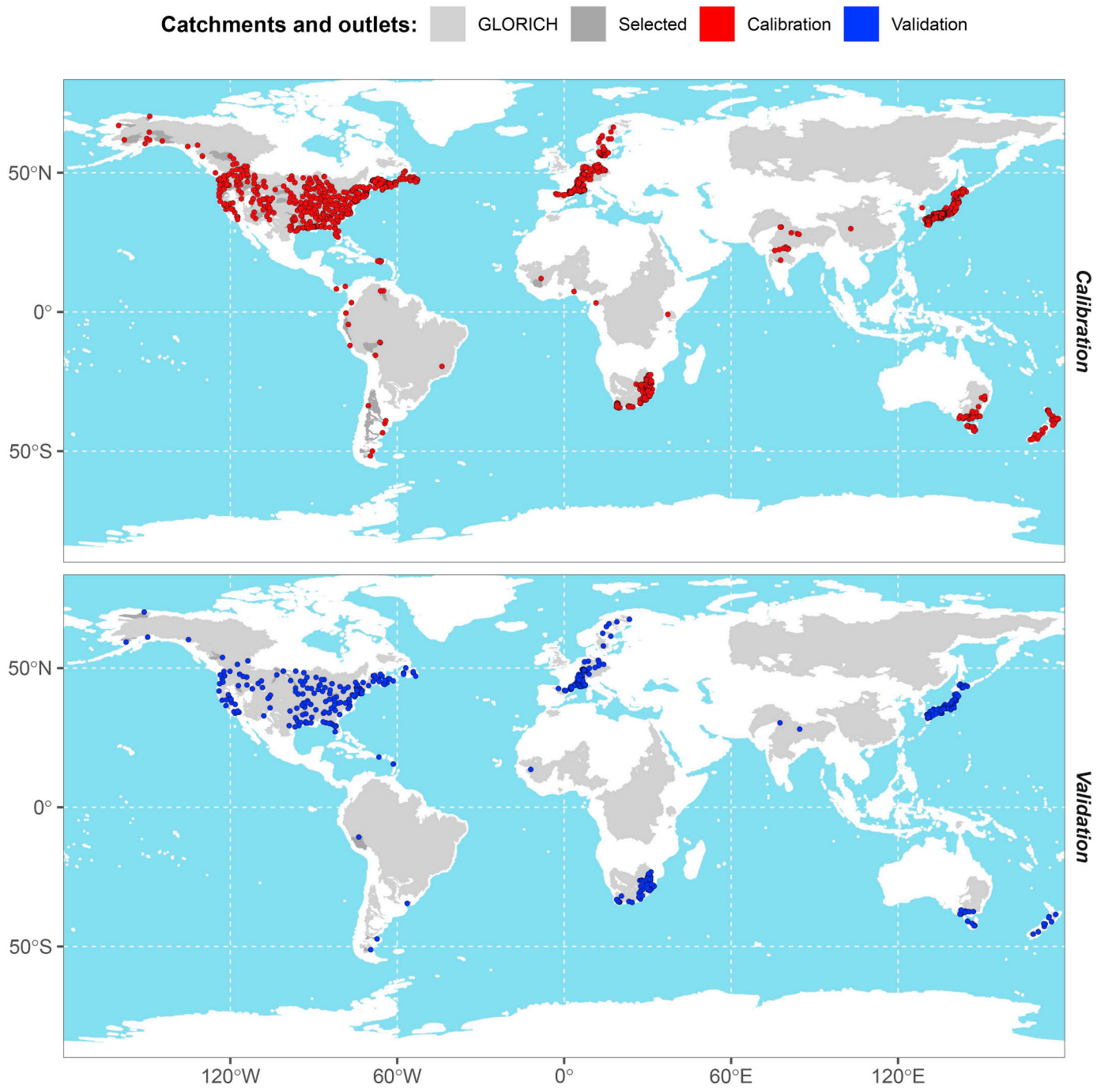

Fig. 2. Original, subset, and classified sampling locations and draining catchments in the present study. Within the original GLORICH dataset (light grey), the darker grey areas represent the selected draining catchments, for which the outlets are represented as red or black points depending on whether they have been used for calibration (n = 1313) or validation (n = 438), respectively. (For interpretation of the references to colour in this figure legend, the reader is referred to the web version of this article.)

The data pre-process resulted in a database with over 180 variables, including chemical fluxes, morphological variables (i.e. altitude, area, slope, etc.), climate variables (monthly and annual temperature, precipitation, windspeed, etc.), land covers (forest, agricultural, managed percentages, etc.), soil types (Leptosols, Cambisols, Nitisols, etc.), soil descriptors (regolith thickness, hydraulic conductivity, pH, etc.), and lithology (Metamorphics, Plutonics Acids and Basics, Carbonate Sedimentary, etc.). This dataset was used to explore the relationships, calibrate the parameters of the equations, and test the residuals of the model created to further define the model.

2.2.4. Database uncertainties

The development, calibration, and validation steps of an empirical model rely on the data used for its construction. In this study, several types of data from different sources were included, selected following an assessment of their quality. Among chemical collection datasets, the GLORICH database (Hartmann et al., 2014b) was chosen because it contained a larger amount of data located in a greater number of catchments. Moreover, it contains two types of data: spot data (related to the samples analysed in each river) and spatial data (relating to the physical description of the draining catchment). Spot data was gathered from different monitoring programs and scientific literature and tested

to eliminate possible errors, although this dataset was considered to have been validated by its creators (Hartmann et al., 2014b). The spatial data for both the GLORICH description of the draining basin characteristics and the added variables is based on contrasted spatial datasets. The lithological distribution was taken from the Global Lithological Map (GLIM, Hartmann and Moosdorf, 2012) which, to the best of the authors' knowledge, is the highest resolution lithological database at a global scale. Soil type abundance was computed using the polygons in the Harmonized World Soil Database (HSWD, FAO et al., 2012). The hydrology was taken from the 0.5°x0.5° raster in the UNH/GRDC Composite Runoff Fields V 1.0 (Fekete et al., 2002). Regolith thickness was taken from the 1x1km raster Global Soil Regolith Thickness (GSDE, Shangguan et al., 2017). Hydraulic conductivity was estimated from the polygons in Global Hydrogeology Maps (GLHYMPS, Huscroft et al., 2018). The seasalt atmospheric deposition was derived from 1°x1° raster from the global assessment of precipitation chemistry (Vet et al., 2014). The uncertainties and limits for each dataset are set out in each of the publications, while in the present analysis the global results are modelled (using the soil, lithology, and specific runoff databases) at a resolution of 0.5°x0.5°.

2.3. Modelling approach

Chemical weathering rates are mainly affected by hydrology, lithology of the underlying bedrock, the overlying soil, and water temperature (Hartmann et al., 2009; Hartmann et al., 2014b). In order to analyse the effect of each one on all of the ion fluxes, it was proposed to test 8 linear equations. To design the equations, a physical interpretation of the estimates was considered, and the variables were added in the following order: lithology, soil shielding effect (further explained in the paragraphs below and in Hartmann et al., 2014b), temperature, hydraulic conductivity and soil depth. The set of equations tested is as follows:

$$F^*_x = q_{ann} \cdot c_x \quad \text{(M1)}$$

$$F^*_x = q_{ann} \cdot \sum (L_i \cdot c_{x_i}) \quad \text{(M2)}$$

$$F^*_x = q_{ann} \cdot f_{s_x}(\text{soil}) \cdot \sum (L_i \cdot c_{x_i}) \quad \text{(M3)}$$

$$F^*_x = q_{ann} \cdot f_T(\text{temperature}) \cdot \sum (L_i \cdot c_{x_i}) \quad \text{(M4)}$$

$$F^*_x = q_{ann} \cdot f_{s_x}(\text{soil}) \cdot f_T(\text{temperature}) \cdot \sum (L_i \cdot c_{x_i}) \quad \text{(M5)}$$

$$F^*_x = q_{ann} \cdot f_D(\text{soil depth}) \cdot \sum (L_i \cdot c_{x_i}) \quad \text{(M6)}$$

$$F^*_x = q_{ann} \cdot f_K(\text{hydraulic conductivity}) \cdot \sum (L_i \cdot c_{x_i}) \quad \text{(M7)}$$

$$F^*_x = q_{ann} \cdot f_{KD}(\text{soil depth} + \text{hydraulic conductivity}) \cdot \sum (L_i \cdot c_{x_i}) \quad \text{(M8)}$$

$$f_{s_x} = \frac{F^*_{x(\text{shield} \geq 0.5)}}{F^*_{x(\text{M2,shield} \geq 0.5)}}$$

$$f_T = \exp\left(\frac{1}{T} - \frac{1}{\overline{T}}\right)$$

$$f_D = \frac{\text{Depth}}{\text{Depth}_{MAX} - b \cdot \text{Depth}}$$

$$f_K = \frac{K_{hyd}}{K_{hyd_{MAX}} - b \cdot K_{hyd}}$$

$$f_{KD} = \frac{\text{Depth}}{K_{hyd}}$$

where F_{x^*} represents the ionic flux derived from chemical weathering of rocks (ICWR) of an element x, measured in mol·m^{-2}·y^{-1}; q_{ann} represents the annual average runoff composite of the catchment (computed as the discharge at the outlet of the catchment over the area of the draining surface), in dm^3·m^{-2}·y^{-1}; L_i accounts for the percentage of the area covered by a lithological group i (see Fig. S6); $f_{s,x}$ is the soil shielding effect factor, dimensionless; f_T represents the temperature effect factor, dimensionless; f_D is the soil depth factor, dimensionless; and the f_K considers the hydraulic conductivity factor, dimensionless; f_{KD} is the soil depth-hydraulic conductivity factor, dimensionless; $F_{x_{sM2}}$ is the flux obtained with model M2, in mol·m^{-2}·y^{-1}; T is the average annual air temperature of the draining basin taken from the GLORICH database, computed from the WordClim (Hijmans, 2019) database, in K; $\overline{T}$ is the global average annual temperature, in K; Depth measures the soil depth, in cm; and K_{hyd} measures the mean hydraulic conductivity, in m·s^{-1}. A further detail of the former three factors is set out in the following paragraphs. For all models tested here, the parameters are c_x, $c_{x,i}$, measured in mol·L^{-1}, and b, dimensionless, and may be interpreted as the average concentration of an element x in the water draining from rock i (c_x and $c_{x,i}$) corrected for atmospheric inputs, and b as the function parameter. The parameters fitted at the calibration step are c_x, $c_{x,i}$, and b.

Soil cover over bedrock has been identified as an important factor to consider when analysing the CW at a global scale (Dupré et al., 2003; Hartmann et al., 2014a). Some soil types with thick profiles, or high organic matter content, or low permeability may act as a buffer to the chemical flux arriving to the river stream, as shown by Boeglin and Probst (1998) for large river basins covered by lateritic soils, where the fluxes of bicarbonates supplied by silicate hydrolysis are half of the river fluxes produced in non-lateric basins. In this regard, Hartmann et al. (2014a) estimated an average soil shielding factor of 0.1 for the following FAO soil types: Ferralsols, Acrisols, Nitisols, Lixisols, Histosols, and Gleysols. Here, we consider a similar factor, but differentiating between the values for each ion. Further explanation is given in Section 2.4. In this study, 416 catchments showed a percentage of coverage of this kind of soil of 50% and were expected to be affected by the "soil shielding effect".

In order to include the soil shielding effect $f_{s,x}$ we established a threshold to differentiate between two groups of catchments: those in which 50% or more of the area was covered by the sum of the soil types Ferralsols, Acrisols, Nitisols, Lixisols, Histosols, and Gleysols (Hartmann et al., 2014a), where the dominance of the soil shielding effect was expected; and those where this sum was under 50%. The mean values of the flux for each group and ion was computed and the ratio of atmospherically corrected observed flux to flux obtained with model M2, for soil-shield-affected affected catchments was computed, giving $f_{s,\ Ca^{2+}} = 0.75$; $f_{s,\ Mg^{2+}} = 0.74$; $f_{s,\ Na^{+}} = 0.46$; $f_{s,\ K^{+}} = 0.78$; $f_{s,\ Alkalinity} = 0.70$; $f_{s,\ SO_4^{2-}} = 0.29$; $f_{s,\ Cl^{-}} = 0.34$.

As regards the temperature effect, catchments with higher average temperature were expected to drain higher fluxes of elements than those with lower temperatures. Annual air temperature was used as a proxy for groundwater mean temperature, which is that responsible for changes in the solubility constants of certain minerals. Then, a similar temperature factor to Hartmann et al. (2014a) with an Arrhenius type equation was then computed as f_T.

2.3.1. Calibration and model evaluation

The parameters from the equations were fitted using a 75% random subset of the data ($n_{calibration} = 1313$) from the selected sites (Fig. 1), while the remainder were used for validation ($n_{validation} = 438$). The fit was carried out using the Levenberg-Marquardt algorithm, a method used to find the minimum of a function, in this case, a sum of squares (Moré, 1978), implemented in the "minpack.lm" package (Elzhov et al., 2010) for the R software (R Core Team, 2018). As the parameters to fit were interpreted as the concentration (c_x, $c_{x,i}$) of an element draining from water from each lithological group, a lower boundary of 0 was established. The performance of the model was evaluated by assessing the significance of the relation between observed and simulated values using Spearman correlation (ρ) and evaluation of the percentage of

Table 1
Spearman correlation coefficients and PBIAS values [%] for the eight models tested here (M1-M8, $n = 1313$) in the calibration dataset. The last column ("MEAN") shows the mean value for all ion assessment in each model. All correlations are statistically significant ($p < 0.01$). M3 is considered the best and analysed further in this text.

	Ca^{2+}		Mg^{2+}		Na^{+}		K^{+}		Cl^{-}		Alkalinity		SO_4^{2-}		MEAN	
	ρ	PBIAS	ρ	PBIAS	ρ	PBIAS	ρ	PBIAS	ρ	PBIAS	ρ	PBIAS	ρ	PBIAS	ρ	PBIAS
M1	0.41	−24.1	0.24	−34.7	0.31	−42.0	0.26	−24.0	0.13	−52.1	0.40	−26.5	0.32	−36.6	0.29	−34.3
M2	0.59	−13.7	0.39	−26.2	0.29	−41.3	0.43	−19.5	0.15	−48.6	0.66	−12.3	0.45	−26.5	0.42	−26.9
M3	0.60	−15.1	0.40	−28.0	0.29	−45.0	0.42	−20.8	0.16	−52.9	0.66	−13.4	0.50	−29.1	0.43	−29.2
M4	0.59	−13.7	0.39	−26.2	0.29	−41.3	0.43	−19.5	0.15	−48.6	0.66	−12.3	0.45	−26.5	0.42	−26.9
M5	0.60	−15.1	0.40	−28.0	0.29	−45.0	0.42	−20.8	0.16	−52.9	0.66	−13.4	0.50	−29.1	0.43	−29.2
M6	0.56	−16.2	0.41	−20.4	0.31	−25.7	0.36	−18.7	0.18	−28.4	0.66	−14.3	0.43	−26.3	0.41	−21.4
M7	0.15	−65.9	0.04	−71.2	0.12	−57.0	0.11	−60.8	0.06	−52.9	0.16	−72.5	0.20	−75.8	0.12	−65.2
M8	0.24	−81.4	0.23	−80.3	0.21	−83.0	0.18	−78.0	0.09	−84.8	0.30	−86.2	0.16	−88.4	0.20	−83.2

deviation (PBIAS), which measures the average tendency of the simulated values to be above or below the observed values.

$$\rho = \frac{\mathrm{cov}(rg_{Observed}, rg_{Simulated})}{\sigma_{rg_{Observed}}\sigma_{rg_{Simulated}}};\ \mathrm{PBIAS} = \frac{\sum (F_{Simulated} - F_{Observed})}{\sum F_{Observed}}$$

where $cov(rg_{Observed}, rg_{Simulated})$ is the covariance of the observed and simulated fluxes, σ_{rg} represents the standard deviation of the variables, and F represents the specific fluxes. Finally, the model is applied over a grid with a cell size of 0.5 × 0.5° where superposition of the GLiM, HSWD, and UNH/GRDC (Fekete et al., 2002) datasets allowed for the generation of single combination cells where the M3 model estimates were applied.

3. Results

3.1. Assessment of model performance

Table 1 summarises the statistics used to evaluate performance of the model, all of which show a significant correlation ($p < 0.01$). M1 only includes the average specific runoff and the fitted parameter represents the average concentration of element x in all catchments; it is used here as a starting point for model performance. As expected, the inclusion of lithology in the regression (M2) improved correlation of the model and decreased the difference between observed and simulated data. Inclusion of the "soil shielding" effect (M3) therefore has improved the correlation but also increased the difference between the data, as shown by the increase in PBIAS. The incorporation of temperature (M4) had no effect when compared to model M2, and neither did the combination of "soil shielding effect" and temperature (M5), while aggregation of soil depth (M6) decreased the correlation with regard to M2 and M3. M7 and M8 show the lowest correlations and the highest PBIAS. It is important to note that there are almost no differences in the statistics from M2 to M5, although the best performance of the model, with the fewest explanatory variables, was achieved with M3, as further analysed in this study.

In general, there is a strong and significant correlation between the median observed and simulated values considering all catchments and ions included in the present study ($r_{Spearman} = 0.96$, $p < 0.01$), as shown in Fig. 3. In addition, both observed and simulated fluxes expand over similar interquartilic ranges (IQR = 3^{rd}Q-1^{st}Q), suggesting that this model configuration is capable of estimating the median and ranges of ionic-specific fluxes in large scale studies.

When each ion is evaluated independently, and site-specific fluxes are compared in observed-simulated pairs, two findings may be derived: there is a higher data scatter, as shown by lower ρ and a greater underestimation of the model, noted by a more negative PBIAS (Table 1). For M3, the best represented ions are Ca^{2+} and Alkalinity, with correlations of over 0.6 and a PBIAS of under 15%, while the poorest are Na^{+} and Cl^{-}, with correlation of under 0.3 and PBIAS >45% (Table 1). Nevertheless, the residuals display a normal distribution, centring on 0, suggesting a valid model configuration.

Application of the model to the validation dataset gives the result shown in Fig. 3b. Like the calibration dataset, the model shows better results for alkalinity, and worse results for Cl^{-}.

3.2. Application of the model

Model M3 has been considered to represent a fair starting point for assessing ICWR at large scales. Before applying it to smaller case studies, it should be contrasted in specific case studies with adapted data, such as observed average specific discharge, soil maps, and lithological distribution, with a finer resolution, instead of using globally derived products. Here, the model is applied to a grid with a cell size of 0.5° where superposition of the GLiM, HSWD, and UNH/GRDC datasets allowed for the generation of single combination cells in which the M3 model estimates were applied. The results of this application are displayed in Fig. 4, which shows the spatial distribution of the ICWR, measured in $Mg{\cdot}km^{-2}{\cdot}y^{-1}$ for easier comparison with previous studies in Table 2.

Overall, higher ICWRs are obtained for alkalinity, SO_4^{2-}, and Ca^{2+}, in concordance with the dominant elements commonly found in freshwater environments, while the lowest ICWRs are found for K^{+}, which commonly accounts for a lower proportion of water chemistry. In general, higher ICWRs are found in latitudes between 15° S and 15° N for all ions, probably related to higher specific discharge and humid tropical climates. This is clearly shown for alkalinity, presenting highest values for the Amazon and the Congo basins, as well as the Polynesian Islands. Low median fluxes are found between 15° N and 30° N and 15° S and 30° S but probably affected by the Saharan and Australian deserts, in contrast, the south-eastern parts of Asia and Central America show higher ICWR. In this study, relevant fluxes are also found between 45° N and 75° N whose contribution to chemical fluxes had previously been assessed as not being relevant (Hartmann et al., 2014a). In the GLORICH database and other input datasets, there is no catchment in the Antarctic and Greenland, though ICWRs in these areas are displayed as No Data, but they are probably affected by snow and ice processes not properly represented in this study, as described by Wadham et al. (2010) and St Pierre et al. (2019).

4. Discussion

4.1. Overall

The present study shows the development of an inverse model for the assessment of ICWR at a global scale, based on aggregated chemical analysis of spot samples at a catchment level around the world, as well as on worldwide datasets. It is the first time that a map of the ionic flux derived from chemical weathering of rocks is presented, and represents an improvement on previously published similar models (Meybeck,

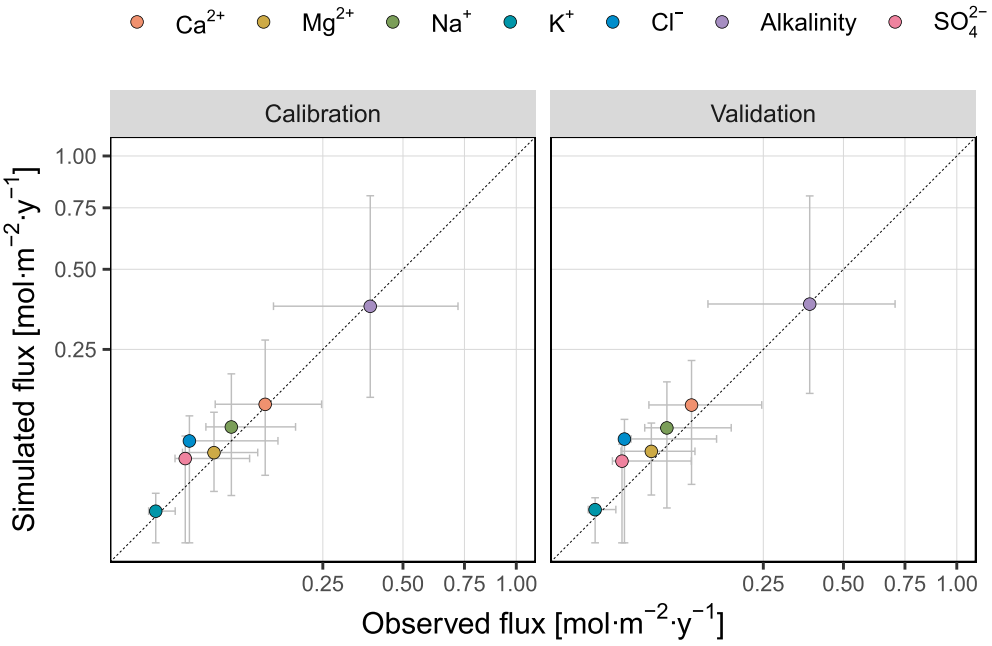

Fig. 3. Scatterplot of simulated and observed data for calibration and validation, using model M3. Each point represents a median value for each ion considered in this study, and the bar expands over the first and third quartiles to show how the average ranges are captured by the model. The dashed line represents 1:1.

1987; Amiotte Suchet and Probst, 1995; Gaillardet et al., 1999; Ludwig et al., 2011; Hartmann et al., 2014a). In order to discuss the results, three main points are established:

- A comparison is made between the results of the model and the last model presented on Chemical Weathering Rates (CWR, Hartmann et al., 2014a) and other global studies, in order to validate the results obtained and contrast the differences.
- A framework of application of this model is established with regard to the spatial scale of application. In addition, the advantages that this configuration poses for potential users, and limitations regarding scales and conceptualization are also discussed.
- An identification and comparison of the hotspots among ions at a global scale is described, to highlight the role of ICWR in global biogeochemical cycles.

4.2. Model validation

The results of the present study are compared to previous studies in Table 2, considering the individual ionic fluxes and their aggregations in cation, anion and total fluxes. In general, the M3 model presents an average global CWR of $\sim 3374 \cdot 10^6$ Mg·y^{-1}, which is lower than previous studies, e.g. $\sim 4175 \cdot 10^6$ Mg·y^{-1} (Meybeck, 1979), $\sim 4050 \cdot 10^6$ Mg·y^{-1} (Probst, 1992), but higher than more recent results $\sim 2131 \cdot 10^6$ Mg·y^{-1} (Gaillardet et al., 1999). However, focusing specifically on the $\sim 734 \cdot 10^6$ Mg ·y^{-1} total cation flux ($\Sigma Z+$), it has a lower value than a recent study at the same scale $\sim 1439 \cdot 10^6$ Mg ·y^{-1} (Hartmann et al., 2014a). Differences in this result are attributed to three main causes: differences in the definition of CWR (inclusion of dissolved silica), the number and location of the reference sampling sites selected for the model calibration step, and the configuration of the model itself. According to results from Meybeck (1979) and Probst (1992), the SiO_2/Ca^{2+} ratio is ~0.7, which would yield a $\Sigma Z^+_{M3_*}$ of $\sim 1034 \cdot 10^6$ Mg·y^{-1} closer to, but lower than, the study by Hartmann et al. (2014a).

The CWR measurement shows discrepancies between research studies, given that several compute the total weathered matter from rocks through Total Dissolved Solids, TDS (e.g. Dessert et al., 2003; Donnini et al., 2016) while others make different aggregations, i.e. cations (e.g. Gaillardet et al., 1999; Dessert et al., 2003; Balagizi et al., 2015) or cations plus SiO_2 (e.g. Hartmann et al., 2014a). In the present study, each ion is computed independently to overcome these discrepancies, in a similar way to Braun et al. (2005) and Goddéris et al. (2009). Among the applications of these studies, a knowledge of CWR is of interest in assessing CO_2 consumption through rock dissolution (Amiotte Suchet and Probst, 1995; Amiotte Suchet et al., 2003; Hartmann et al., 2009), in studying the global biogeochemical cycles of P (c.f. Hartmann et al., 2014a), and in characterising the riverine end-member in oceanic assessments (Sun et al., 2016). Assessing each ion independently offers an opportunity for a more detailed description of the CW process and the associated assessments at a global scale. In this regard, the present study will be a reference for future works, especially in large-scale applications (see discussion sections below). The ICWR model yields similar flux median and ranges values as compared to the observed data for alkalinity, but a poorer representation of Cl^-, linked to a predominantly atmospheric input and traces of evaporites located in other lithological groups that are not large enough to be mapped at a global scale but are large enough to have a significant impact on riverine loads.

Previous authors have attributed the overestimation of empirically-modelled CWR in tropical areas (such as the Amazon, Congo, and Orinoco basins) and its underestimation in northern latitudes to the small number of sampling locations included in development of the model (see discussion in Hartmann et al., 2014a and Goddéris et al., 2006). The recent study by Hartmann et al. (2014a) extrapolated a regionally fitted model (using 381 sampling locations in the Japanese Archipelago, see Hartmann and Moosdorf, 2011) to the world, and further refined its formulation by considering 49 large river catchments in different locations worldwide, among which there are several tropical and Arctic basins. Gaillardet et al. (1999), on the other hand, initially included this kind of basin in their model fitting, taking the 60 largest rivers in the world as a reference. Here, 1313 sampling locations in large basins and small catchments in warm and cold climates around the world were used for the model fit step, reflecting greater variability in the parameter estimates and thus giving to more robust results, as supported by the residual normal distribution.

Nevertheless, even though the number of sampling locations is greater than in previous empirical model developments, they are

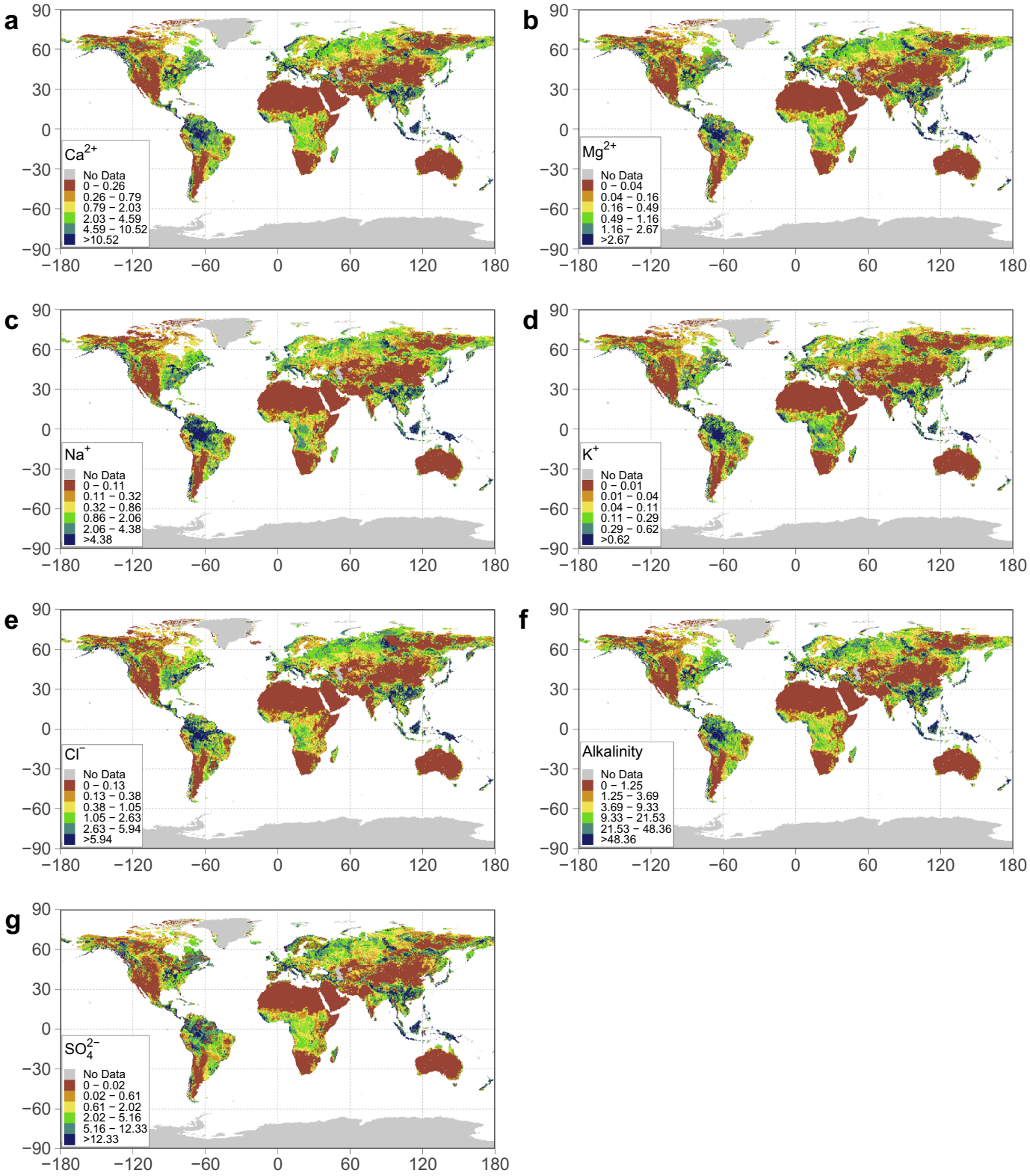

Fig. 4. Holospheric distribution of Ionic fluxes derived from Chemical Weathering of Rocks (ICWR), all data expressed in $Mg{\cdot}km^{2}{\cdot}y^{-1}$. The maps were obtained by applying the model to a global grid of 0.5° using the fitted parameters in model M3. Note that each ion presents a different colour range based on the global percentile distribution, using $P10^{th}$, $P25^{th}$, $P50^{th}$, $P75^{th}$, and $P90^{th}$ as breakpoints.

spatially clustered in some areas, excluding relevant areas from the calibration and validation steps (Fig. 3). Northern latitudes (the Arctic catchments), Polynesian sampling locations and a large quantity of data available from Asia are not included in the present analysis because of non-availability in the data source selected, or due to the subset criterion established (see Section 2.2.1). Despite not including these areas, the calibration subset is considered to be representative of different climates, soils and lithological characteristics (see Supplementary

Table 2
Comparison between studies on of CWR at global scales. All values expressed at 10^6 Mg·y^{-1}. ΣZ^+ represent the Ca^{2+}, Mg^{2+}, Na^+, and K^+ while ΣZ^- for Cl^-, SO_4^{2-}, and Alkalinity (expressed as HCO_3^-). Bracketed values represent a recalculation of ΣZ^+ adding a virtual contribution of SiO_2, considering a SiO_2/Ca^{2+} of 0.7.

Study	Code	Ca^{2+}	Mg^{2+}	Na^+	K^+	Alkalinity	SO_4^{2-}	SiO_2	Cl^-	ΣZ^+	ΣZ^-	Total flux from Chemical Weathering
This study	M1	374	100	223	25	1815	401	–	246	722 (984)	2462	3184 (3446)
	M2	484	121	202	29	2234	500	–	263	836 (1175)	2997	3833 (4172)
	M3	428	107	176	24	1954	465	–	221	734 (1034)	2640	3374 (3674)
	M4	527	132	221	31	2434	545	–	287	911 (1284)	3266	4177 (4550)
	M5	477	119	202	27	2139	490	–	241	825 (1159)	2870	3695 (4029)
Meybeck (1979)	Natural	502	126	192	48	1940	307	–	215	868	2462	3330
	Total	549	136	270	53	2040	431	388	308	1008	3167	4175
Probst (1992)		510	141	211	73	2013	455	355	223	935	3046	3981
Gaillardet et al. (1999)		–	–	–	–	–	–	–	–	–	–	2131
Hartmann et al. (2014a)	Soil shielding applied	–	–	–	–	–	–	–	–	(1439)	–	–

Information, Figs. S3-S7), allowing a flexible tool to be developed that is capable of capturing a great variability in catchment characteristics, albeit acknowledging its limitations (see Section 4.3 Domain of application).

CW of rocks is a complex process that is controlled by several factors that vary with soil depth, e.g. the composition of minerals (Apollaro et al., 2019; Biondino et al., 2020), and the hydrology (Gabet et al., 2006; Anderson et al., 2004; Hartmann, 2009). Boeglin and Probst (1998) showed that for large river basins, the atmospheric/soil CO_2 consumed by silicate weathering and the associated bicarbonate river fluxes are 1.8 times lower when the bedrock is covered by deep lateritic soils. Oliva et al. (2003) noted that regolith depth shields the rocks from CW in areas where this layer is thicker, however Dong et al. (2018) reported that the highest CW occurs at an intermediate soil thickness. In this regard, we hypothesized that a larger regolith (soil + saprolite) layer would act as a proxy for erosion-product deposition, and in synergy with a low hydraulic conductivity, would result in a lower CWR (Gabet et al., 2006; Anderson et al., 2004).

However, inclusion of global regolith thickness (Shangguan et al., 2017) and hydraulic conductivity (Huscroft et al., 2018) in this study did not improve the results. We associate this finding with the model configuration and the scale of application. In addition, the GLHYMPS database (Huscroft et al., 2018) was computed from the GLiM database, which is already accounted in the model variables, although information may already have been included in the lithological group classification. In contrast with our study, Dong et al. (2018) succeeded in including of these variables using a physically based model, by making a distinction between different soil layers. However, our data-driven model was not capable of including these variables within its context and the area of application poses a challenge in describing the required variables. Nonetheless, an improvement in performance of the model in relation to soil data can be found in the "soil shielding effect" factor (Dupré et al., 2003; Hartmann et al., 2014a), computed for soil types classified based on their pedogenesis in the HSWD database (FAO et al., 2012). Soils with thick layers, low hydraulic conductivities, dominated by organic matter decay, or with a shallow ground water table (Hartmann et al., 2014a) would have a stronger shielding effect. We attribute the improvement in the model's results to the soil shielding effect, and the lack of success in including new variables to the fact that the combination of the lithological and soil classification maps already takes into account the interaction of chemical fluxes with the soil layers overlying the bedrock zone, and the fact that the inclusion of regolith thickness and hydraulic conductivity requires a physically-based approach for inclusion in studies of chemical weathering studies.

Temperature is another variable initially considered to be relevant in CW (Drever and Zobrist, 1992, Dessert et al., 2003, Hartmann et al., 2014), since it reflects changes in the equilibrium constant of the dissolution reactions (Drever, 2012). An increase in water temperature would increase dissolution of rocks and augment biological activity, through respiration and pCO_2 in the soil, but it would also reduce the gas dissolution in the liquid. However, CO_2 is produced by ecosystem respiration, inducing acids responsible for chemical weathering; this is a two-factor dependence (soil water content and temperature) which explains why an Arrhenius-type factor for the model alone does not improve the results (Romero-Mujalli et al., 2019). Dissolution takes place in the regolith water and groundwater but we could find no database with worldwide spatially distributed temperature values. For this reason, air temperature is used as a proxy for this effect, but its inclusion does not provide any improvement in the model. This is related to two main factors: the different effect on the dissolution of each mineral and that the fact that, although groundwater temperature is dependent on annual average air surface temperature, this variable appears not to be a proxy related to the temperature effect on CW reactions. Further research is needed to analyse the effect of water temperature on these fluxes worldwide.

At the conceptualization stage (see Section 2.1), several other variables were considered, such as vegetation (land cover), evapotranspiration, or a finer definition of rocks (including rock ages), but after some consideration, these data were not included in the development stage. Vegetation fixes atmospheric C through photosynthesis, which is later exchanged by roots with microorganisms during soil respiration, increasing the CO_2 concentration in the soil pores, which would dissolve in water to generate carbonic acid and enhance rock dissolution, thus releasing ions into the water matrix (c.f. Keller, 2019). However, changes in the photosynthesis process, soil respiration and evapotranspiration are processes with a higher variability (posing a challenge in modelling them, c.f. Chen and Liu, 2020) than the annual mean value used in this study, although this variability could not be captured. Evapotranspiration, conditioned by climatic variables such as temperature and precipitation, affects the water balance by extracting water from the system (i.e. basin) causing an increase in the saline concentration found in rivers. However, its effect on CW is less pronounced than other characteristics, such as lithological classification (White and Blum, 1995). This suggests that a better representation of the effect of precipitation, air temperature and other climatic variables on chemical weathering rates is mainly related to an improvement in the water balance at a basin scale, which could be achieved by using more detailed models. Lastly, in comparison with previous similar studies (Meybeck, 1986; Amiotte Suchet and Probst, 1995) recent studies include a larger number of lithological classes (Hartmann et al., 2014b, this study), involving a finer definition of minerals. Despite this larger number, further levels of classification of lithologies are available (c.f. Hartmann and Moosdorf, 2012), but given the number of sampling locations, it would have been a challenge to include all of them, as most of them would not vary in a wide enough range to calibrate the parameters in the model. Even with the classification used in this study, there are some lithological classes which do not span the entire spectrum (e.g. plutonic intermediate, see Supplementary Information, Fig. S6), meaning that in the subset considered in this study, there are no catchments in which 100% of the draining area is covered by these lithologies. The inclusion of finer lithological classification should focus on smaller-scale cases, where mechanistic models may be applied, or

when the chemical data compilation includes cases spanning the entire range of values.

Despite the current assessment, the relative importance of these variables in chemical weathering may not be well represented in the selected modelling approach, since data-driven models describe the process based on correlations of the data and not on physical fundaments, as mechanistic models do (e.g. WITCH model, Goddéris et al., 2006). The uncertainty regarding this kind of model is large and difficult to quantify (Hartmann et al., 2014a), and is strongly affected by the reference sampling locations and the pre-processing step, which may induce bias in the data used for model fitting. Strict criteria on sampling location selection excludes around 80% of the data included in the original database but excludes the bias introduced by isolated samples (catchments sampled only once or twice) or from heavily anthropogenically affected samples.

The greatest uncertainty in the pre-processing step is found in the separation of the riverine flux between atmospheric and bedrock fluxes, but its relevance is noted in previous literature (Stallard and Edmond, 1981; Meybeck, 1986; Dessert et al., 2003; Hartmann and Moosdorf, 2011). With regard to the ionic sources in streams, atmospheric deposition has been noted as being relevant with regard to the input of sea-salt derived Cl^- and Na^+, especially in catchments located close to the coast (Meybeck, 1986; Berner and Berner, 2012). In arid regions, the atmospheric input of Ca^{2+} and K^+ is related more to aeolian dust, biomass burning, or industrial emissions (Vet et al., 2014). Several publications show large scale deposition of base ions in the United States (e.g. Brahney et al., 2013) and other authors such as Lehmann et al. (2005) have studied the temporal evolution of these depositions. In this study, no temporal evolution has been studied, but an average spatial value has been derived from the data of Vet et al. (2014), which may differ for specific cases and requires further analysis when downscaling the model.

To the best of the authors' knowledge, no results of mechanistic models representing ICWR at a global scale have previously been published, as upscaling of this kind of models is constrained to the data availability (creating a need for assumptions or simplifications when applying to large scales) and computing resources. In this context, the present study represents a step forward in the assessment, through modelling, of CW at a global scale in three main aspects: assessing CW at a global scale making a distinction of each ion; establishing a simple law that can be downscaled to catchment-level studies in later studies, and highlighting the need for physically-based principles in order to study the effect of variables such as regolith thickness, hydraulic conductivity, or water temperature.

4.3. Domain of application

In general, this kind of model has been applied at regional or global scale to perform several assessments, such as atmospheric CO_2 sequestration by rocks through dissolution of minerals (Probst, 1992; Amiotte Suchet and Probst, 1995; Amiotte Suchet et al., 2003; Ludwig et al., 1998; Balagizi et al., 2015), Si mobilization (Jansen et al., 2010) and analysis of the P-release (Hartmann et al., 2014a). Alkalinity fluxes measured in rivers have commonly been used as a tracer of CO_2 sequestration by CW, and two main groups of rocks have been studied: carbonates and silicates. Following the reactions shown in Fig. S1, alkalinity fluxes from silicate rocks come only from the atmospheric/soil CO_2, while for carbonates draining waters, 50% of the riverine flux is associated with lithogenic carbonate contribution (Amiotte Suchet and Probst, 1993a; Probst et al., 1994; Gaillardet et al., 1999; Hartmann et al., 2009; Balagizi et al., 2015). It is important to note that SiO_2 is not considered in this study, because its implication for the biogeochemical cycle is strongly affected by its accumulation on amorphous silica, or biogenic silica in living organisms (Conley, 2002) processes which proved complex to simulate at the present scale.

Here, the present model defines the CWR by its constituents, i.e. ions, analyses the weight of each one in the total flux and helps to assess the average specific flux. The poor representation of Na^+ fluxes is linked to different drivers governing the dissolution of the rocks with this kind of elements, such as albite or volcanic glass, which are reported as large CO_2 sinks in a global context (Dessert et al., 2003). In order better to represent the Na^+ and SO_4^{2-} ions from an inverse modelling point of view, other variables should be taken into consideration, as their presence may be linked more to redox processes than to congruent dissolution by acids (Berner and Berner, 2012), like dissolved oxygen concentration or redox potential, which are commonly measured in the field. This finding highlights the importance of analysing all ions when considering CW and other associated processes, as since although the CWR has previously been quantified, the representation of all ions in this flux is not equally well defined, indicating that further research is needed to improve the representation of those elements and an understanding of the associated processes. Keller (2019) shows an analysis of the Critical Zone and explains CW in its context; a relevant number of variables are tied up with this process (including denudation rate, rock age, etc.), and these variables should be taken into consideration in any further developments of these models and may be responsible for the variability not captured by the model. This study has shown that CWR is mostly conditioned by Ca^{2+} and alkalinity, though the other ions need further research to be properly represented.

A relevant factor in applying this model is the scale of application. The model has been applied at a global scale, but the initial data encapsulated catchments with different sizes. In general, basins draining an area between 10 and 10,000 km^2 were those that showed discrepancies of within ±20% between modelled and observed data (Table S3). Those two limits encompass most of the catchments considered in this study and are therefore, the best spatial scale for application of the model. Larger catchments are expected to drain water affected by more processes other than CW (such as cyclic salts and pollution) and have a more complex hydrology, while smaller catchments may not be well defined in terms of the lithological composition. A compromise between the scale of application and the level of detail needs to be found in order to apply a model, especially for large scale applications (Fu et al., 2019). This is a limitation for application of the model at this step; further analysis on the performance and variability captured by the model in larger or smaller catchments should be studied and considered in future studies.

In addition to the applications noted above, the model provides an opportunity to assess the natural major ionic composition of water, relevant in analysis of crop production (Wicke et al., 2011) and useful when analysing “river syndromes” (salinization, eutrophication, etc. see Meybeck, 2003) at the scales indicated. An initial snapshot for ICWR fluxes is presented in Fig. 4. This data can be used as a reference for scarce data availability on water chemistry analysis and as a constraint for assessing anthropogenic influence in analysis of catchment water. Moreover, the method presented can be used as a guide for developing models with different lithological classifications if a different the lithological map exists, and enough data are available for parameter fitting.

Application of this model is tested for sampling locations with the characteristics summarised in the Supplementary Material (Figs. S3-S7) and extrapolation of the model to a global scale yielded to a similar value to recent studies (see Section 4.2). Nonetheless, constraints have been found for classification of the lithology and soil considered in the input dataset (see Figs. S6 and S7 for a summary). Temporal evolution has not been tested, as chemical data was summarised to a unique value per catchment, and hydrology was aggregated to a single annual value. Refinement of the model should focus on distinguishing the different hydrological fluxes (groundwater, surface, lateral flows, etc.) in order to take into account processes of dilution and concentration, apart from the improvements in representation of the CW process. As regard performance of the model, the main limitation of this model is the poorer

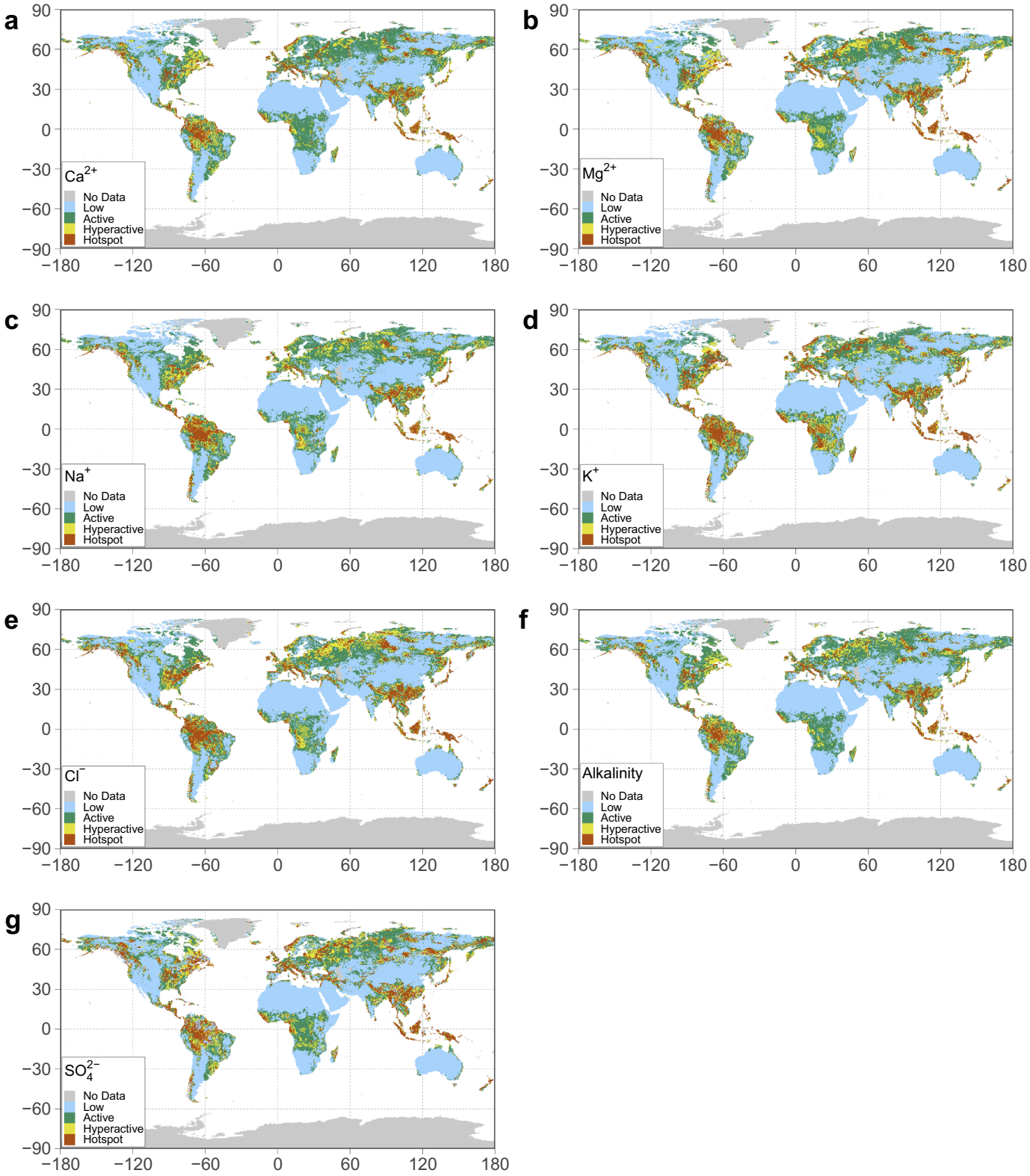

Fig. 5. Holospheric distribution of low, active, hyperactive, and hotspot areas with regard to ICWR at a global scale. The classification is based on the global median value. Low activity areas (blue) are those that stand below the median global ICWR; Active areas (green) contain areas between the median and 5 times the median global ICWR; Hyperactive areas (yellow) include areas with between 5 and 10 times the global ICWR; and Hotspots (red) are those with over 10 times the global median value. (For interpretation of the references to colour in this figure legend, the reader is referred to the web version of this article.)

representation of some ions (Na^+ and Cl^-) compared to others (Ca^{2+} and alkalinity).

4.4. Hotspots at a global scale

Previous literature (McClain et al., 2003) has called for an assessment of hotspots and hot moments in the study of biogeochemical cycles. Although the present analysis does not take temporal evolution into account, the results shown in Fig. 4 may be used to assess relevant spatial locations with regard to the CW of the different ions, on which future research should focus. Taking the classification u sed in Hartmann et al. (2009) as a starting point, four zones have been established for inter- comparison between ions: low zones, where the ICWR is at most the global median value; active zones, where ICWRs range from the median value to five t imes t he m edian v alue; hyperactive areas, where ICWRs range from five t o t en t imes t he median value; and hotspots, where ICWR crosses the median- x- 10 threshold (Fig. 5). In general, hotspots are located between 30° N and 30° S in the northern part of South America, Central America, south- eastern Asia and the Polynesian islands. They are also common in the north-west and eastern part of North America, Central Europe and some areas in northern Asia, New Zealand and the south- western part of South America. These hot- spot are located in higher specific r unoff areas (Fekete et al., 2002), mainly in tropical and temperate areas (Beck et al., 2018), which explain higher fluxes, but they are also linked to Acrisol, Ferralsol, Gleysol, Histosol, Lixisol, and Nitisol soils (FAO et al., 2012) which shield the underlying rocks from CW. The presence of soil shielding classes and the different effects fo und for e ach io n may explain the different s patial p atterns a mong i ons w ithin t hese areas, especially noted for Na^+, Cl^-, and SO_4^{2-} (Fig. 5).

A discussion of CW rates in northern latitudes, islands and areas of volcanic arcs may be found in Hartmann et al. (2014a), which were found to be highly active with regard to chemical weathering rates. Such active areas in the northern latitudes (specially for Ca^{2+}, Mg^{2+}, and alkalinity) may be related to highly weatherable carbonate material, most common between 20° N and 50° N (Amiotte Suchet et al., 2003). The results of the present analysis support the maintenance of these areas as hotspots; however, differences were found between ions. The Congo basin contains several hotspot areas for Na^+, K^+, and Cl^-, related to areas with evaporitic presence or soils with lower shielding effect which are less present for Ca^{2+}, Mg^{2+}, or alkalinity. Similarly, hotspots for these ions are also found in the interior of the Amazon basin, which result from a high specific runoff in this area. In contrast, field s tudies i n t he A mazon b asin (e.g. M oquet e t a l., 2 016) have highlighted the role of the Andean mountain belt in the delivery of dissolved solutes in this tropical catchment, in opposition to the lowland area. In the present study, low active areas in the Andes are related to an underestimation of the specific discharge in these areas, which has previously been noted (Hartmann et al., 2014a). In contrast to the Andean mountain belt, the Himalayas are classified as hotspots for all ions considered in this study. The reasons for these differences in comparison to the study by Hartmann et al. (2014a) may be explained by considering each ion independently for the establishment of ICWR and differentiating t he s oil s hielding e ffect am ong el ements. These findings suggests that, although CWR at a global scale may be dominated by alkalinity and Ca^{2+} because of their higher magnitudes, the contribution of each ion should be considered independently, since the implications for other biogeochemical cycles (C sequestration through CW, riverine end-member characterization regarding saline inputs, or land-ocean loadings) could be better delimited by considering this approach.

5. Conclusions and further developments

This study presents an assessment of the global ICWR for the major ions Ca^{2+}, Mg^{2+}, K^+, Na^+, SO_4^{2-}, Cl^- and alkalinity, together with its spatial distribution. Overall, although this kind of model contains an important degree of uncertainty, this study contributes to a closer step between empirical and mechanical approaches, since it improves the representation of CWR by separating the total fluxes into ionic fluxes (ICWR); it is based on a broader collection of sampling locations, and it has taken into consideration up-to-date worldwide databases, highlighting better representation of ions such as Ca^{2+} and alkalinity, and poorer representation of Na^+ and Cl^-. The results of this analysis indicate that a regression including lithology, soil and hydrology is enough to estimate the average flux and ranges of major ion CWR at a global scale. The results also show that previous measurements of CWR are mainly determined by Ca^{2+} and alkalinity, though the other elements need to be analysed to understand the key variables dominating their geochemical cycles at a global scale. This study also supports the idea that the most relevant factors are lithological distribution, hydrological representation and the soil shielding effect. In contrast, temperature was not concluded as to be relevant, but its role remains uncertain. In addition, the results coincide with previous identification of hotspots in temperate climate latitudes but reflect the importance of considering more northerly latitudes in global matter assessments. Further studies should focus on improving representation of the input data, as well as a more in-depth analysis the worst represented ions, and a shift in approach from a static model to a dynamic approach, considering the changes on these fluxes over time, and thus allowing forecasting studies to be applied.

Acknowledgements

The authors wish to thank the Basque Government (Consolidated Group IT 1029–16), the University of the Basque Country (UPV/EHU) (UFI 11/26), and the Institut National Polytechnique de Toulouse (INPT) for supporting this project. In addition, the authors are grateful to the donors of the global data used in this study, including Prof. Fekete, Dr. Vörosmarty and Dr. Grabs for the UNH/GRDC database, Prof. Shangguan for the GSDE dataset, Jordan Huscroft for the GLHYMPS database, and to the World Data Centre for Precipitation Chemistry, for the atmospheric deposition dataset, as well as all the collaborators in producing these datasets. Jens Hartmann was supported by the Deutsche Forschungsgemeinschaft (DFG, German Research Foundation) under Germany's Excellence Strategy – EXC 2037 'Climate, Climatic Change, and Society' – Project Number: 390683824, and contributes to the Center for Earth System Research and Sustainability (CEN) of the Universität Hamburg. The authors declare no conflict of interest. In addition, the authors wish to thank two anonymous reviewers for providing helpful comments on earlier drafts of the manuscript

Declaration of Competing Interest

The authors declare that they have no known competing financial interests or personal relationships that could have appeared to influence the work reported in this paper.

Appendix A. Supplementary data

Supplementary data to this article can be found online at https://doi.org/10.1016/j.gloplacha.2020.103226.

References

Amiotte Suchet, P., Probst, J.L., 1993a. Flux de CO_2 consommé par altération chimique continentale: influences du drainage et de la lithologie. Comptes Rendus de l'Académie des Sciences de Paris 317, 615–622.

Amiotte Suchet, P., Probst, J.L., 1993b. Modelling of atmospheric CO_2 consumption by chemical weathering of rocks: Application to the Garonne, Congo and Amazon basins. Chem. Geol. 107 (3–4), 205–210. https://doi.org/10.1016/0009-2541(93)90174-H.

Amiotte Suchet, P., Probst, J.L., 1995. A global model for present-day atmospheric/soil

CO_2 consumption by chemical erosion of continental rocks (GEM-CO2). Tellus B 47 (1–2), 273–280.
Amiotte Suchet, P., Probst, J.L., Ludwig, W., 2003. Worldwide distribution of continental rock lithology: Implications for the atmospheric/soil CO_2 uptake by continental weathering and alkalinity river transport to the oceans. In *Global Biogeochem*. Cycles 17 (2), 7/1–7/13. https://doi.org/10.1029/2002GB001891.
Anderson, Suzanne P., Blum, J., Brantley, S.L., Chadwick, O., Chorover, J., Derry, L.A., et al., 2004. Proposed initiative would study Earth's weathering engine. EOS, Transactions, American Geophysical Union 85 (28), 265–272.
Apollaro, C., Perri, F., Le Pera, E., Fuoco, I., Critelli, T., 2019. Chemical and minero-petrographical changes on granulite rocks affected by weathering processes. Frontiers of Earth Science 13 (2), 247–261. https://doi.org/10.1007/s11707-018-0745-5.
Balagizi, C.M., Darchambeau, F., Bouillon, S., Yalire, M.M., Lambert, T., Borges, A.V., 2015. River geochemistry, chemical weathering, and atmospheric CO_2 consumption rates in the Virunga Volcanic Province (East Africa). Geochem. Geophys. Geosyst. 16 (8), 2637–2660. https://doi.org/10.1002/2015GC005999.
Beck, H.E., Zimmermann, N.E., McVicar, T.R., Vergopolan, N., Berg, A., Wood, E.F., 2018. Present and future Köppen-Geiger climate classification maps at 1-km resolution. Scientific Data 5, 180214. https://doi.org/10.1038/sdata.2018.214.
Berner, E.K., Berner, R.A., 2012. Global Environment. Water, Air, and Geochemical cycles, 2nd ed. Princeton.
Biondino, D., Borrelli, L., Critelli, S., Muto, F., Apollaro, C., Coniglio, S., ... Perri, F., 2020. A multidisciplinary approach to investigate weathering processes affecting gneissic rocks (Calabria, southern Italy). CATENA 187, 104372. https://doi.org/10.1016/j.catena.2019.104372.
Boeglin, J.L., Probst, J.L., 1998. Physical and chemical weathering rates and CO_2 consumption in a tropical lateritic environment: the upper Niger basin. Chem. Geol. 148, 137–156. https://doi.org/10.1016/S0009-2541(98)00025-4.
Brahney, J., Ballantyne, A.p., Sievers, C., Neff, J.C., 2013. Increasing Ca^{2+} deposition in the western US: the role of mineral aerosols. Aeolian Res. 10, 77–87. https://doi.org/10.1016/j.aeolia.2013.04.003.
Braun, J.J., Ngoupayou, J.R.N., Viers, J., Dupré, B., Bedimo Bedimo, J.-P., Boeglin, J.-L., ... Muller, J.-P., 2005. Present weathering rates in a humid tropical watershed: Nsimi, South Cameroon. Geochimica et Cosmochimica Acta 69 (2), 357–387. https://doi.org/10.1016/j.gca.2004.06.022.
Carey, R.O., Migliaccio, K.W., 2009. Contribution of wastewater treatment plant effluents to nutrient dynamics in aquatic systems: a review. Environ. Manag. 44 (2), 205–217. https://doi.org/10.1007/s00267-009-9309-5.
Chen, J.M., Liu, J., 2020. Evolution of evapotranspiration models using thermal and shortwave remote sensing data. Remote Sens. Environ. 237, 111594. https://doi.org/10.1016/j.rse.2019.111594.
Conley, D.J., 2002. Terrestrial ecosystems and the global biogeochemical silica cycle. Global Biogeochemical Cycles *16* (4), 68-1–68-8. https://doi.org/10.1029/2002GB001894.
Dailey, K.R., Welch, K.A., Lyons, W.B., 2014. Evaluating the influence of road salt on water quality of Ohio rivers over time. Applied Geochemistry 47, 25–35. https://doi.org/10.1016/j.apgeochem.2014.05.006.
Dessert, C., Dupré, B., Gaillardet, J., François, L.M., Allègre, C.J., 2003. Basalt weathering laws and the impact of basalt weathering on the global carbon cycle. Chem. Geol. 202 (3–4), 257–273. https://doi.org/10.1016/j.chemgeo.2002.10.001.
Di Figlia, M.G., Bellanca, A., Neri, R., Stefansson, A., 2007. Chemical weathering of volcanic rocks at the island of Pantelleria, Italy: Information from soil profile and soil solution investigations. Chem. Geol. 246 (1–2), 1–18. https://doi.org/10.1016/j.chemgeo.2007.07.025.
Dong, X., Cohen, M.J., Martin, J.B., McLaughlin, D.L., Murray, A.B., Ward, N.D., et al., 2018. Ecohydrologic processes and soil thickness feedbacks control limestone-weathering rates in a karst landscape. *Chemical Geology*. https://doi.org/10.1016/j.chemgeo.2018.05.021.
Donnini, M., Frondini, F., Probst, J.L., Probst, A., Cardellini, C., Marchesini, I., Guzzetti, F., 2016. Chemical weathering and consumption of atmospheric carbon dioxide in the Alpine region. Global and Planetary Change 136, 65–81. https://doi.org/10.1016/j.gloplacha.2015.10.017.
Drever, J.I., 2012. The Chemistry of Weathering. Springer Science & Business Media.
Drever, J.I., Zobrist, J., 1992. Chemical weathering of silicate rocks as a function of elevation in the southern Swiss Alps. Geochim. Cosmochim. Acta 56 (8), 3209–3216. https://doi.org/10.1016/0016-7037(92)90298-W.
Dupré, B., Dessert, C., Oliva, P., Goddéris, Y., Viers, J., François, L., et al., 2003. Rivers, chemical weathering and Earth's climate. Compt. Rendus Geosci. 335 (16), 1141–1160. https://doi.org/10.1016/j.crte.2003.09.015.
Elzhov, T.V., Mullen, K.M., Bolker, B., 2010. R interface to the Levenber-Marquardt nonlinear least-squares algorithm found in MINPACK: R package version 1.2-1. Retrieved from. https://CRAN.R-project.org/package=minpack.lm.
FAO, IIASA, ISRIC, ISS-CAS, JRC, 2012. Harmonized World Soil Database. Version 1.2. FAO, Rome, Italy and IIASA, Laxenburg, Austria.
Fekete, B.M., Vörösmarty, C.J., Grabs, W., 2002. High-resolution fields of global runoff combining observed river discharge and simulated water balances. Global Biogeochemical Cycles 16 (3), 15–1–15–10. https://doi.org/10.1029/1999GB001254.
Fu, B., Merritt, W.S., Croke, B.F.W., Weber, T.R., Jakeman, A.J., 2019. A review of catchment-scale water quality and erosion models and a synthesis of future prospects. Environ. Model Softw. 114, 75–97. https://doi.org/10.1016/j.envsoft.2018.12.008.
Gabet, E.J., Edelman, R., Langer, H., 2006. Hydrological controls con chemical weathering rates at the soil-bedrock interface. Geology 34 (12), 1065–1068. https://doi.org/10.1130/G23085A.1.
Gaillardet, J., Dupré, B., Louvat, P., Allègre, C.J., 1999. Global silicate weathering and CO_2 consumption rates deduced from the chemistry of large rivers. Chem. Geol. 159, 3–30. https://doi.org/10.1016/S0009-2541(99)00031-5.
Galloway, J.N., Dentener, F.J., Capone, D.G., Boyer, E.W., Howarth, R.W., Seitzinger, S.P., ... Vörösmarty, C.J., 2004. Nitrogen Cycles: Past, Present, and Future. Biogeochemistry 70, 153–226. https://doi.org/10.1007/s10533-004-0370-0.
Garrels, R.M., Mackenzie, F.T., 1972. A quantitative model for the sedimentary rock cycle. Mar. Chem. 1, 27–41. https://doi.org/10.1016/0304-4203(72)90004-7.
Gibbs, R.J., 1970. Mechanisms Controlling World Water Chemistry. Science 170, 1088–1090.
Goddéris, Y., François, L.M., Probst, A., Schott, J., Moncoulon, D., Labat, D., Viville, D., 2006. Modelling weathering processes at the catchment scale: the WITCH numerical model. Geochim. Cosmochim. Acta 70 (5), 1128–1147. https://doi.org/10.1016/j.gca.2005.11.018.
Goddéris, Y., Roelandt, C., Schott, J., Pierret, M.C., François, L.M., 2009. Towards an Integrated Model of Weathering, climate, and Biospheric Processes. Rev. Mineral. Geochem. 70 (1), 411–434. https://doi.org/10.2138/rmg.2009.70.9.
Guo, J., Wang, F., Vogt, R.D., Zhang, Y., Liu, C.-Q., 2015. Anthropogenically enhanced chemical weathering and carbon evasion in the Yangtze Basin. Sci. Rep. 5, 11941. https://doi.org/10.1038/srep11941.
Hartmann, J., 2009. Bicarbonate-fluxes and CO_2-consumption by chemical weathering on the Japanese Archipelago — Application of a multi-lithological model framework. Chem. Geol. 265 (3–4), 237–271. https://doi.org/10.1016/j.chemgeo.2009.03.024.
Hartmann, J., Moosdorf, N., 2011. Chemical weathering rates of silicate-dominated lithological classes and associated liberation rates of phosphorus on the Japanese Archipelago—Implications for global scale analysis. Chem. Geol. 287 (3–4), 125–157. https://doi.org/10.1016/j.chemgeo.2010.12.004.
Hartmann, J., Moosdorf, N., 2012. The new global lithological map database GLiM: a representation of rock properties at the Earth surface. Geochem. Geophys. Geosyst. 13 (12). https://doi.org/10.1029/2012GC004370.
Hartmann, J., Jansen, N., Dürr, H.H., Kempe, S., Köhler, P., 2009. Global CO_2-consumption by chemical weathering: what is the contribution of highly active weathering regions? Glob. Planet. Chang. 69 (4), 185–194. https://doi.org/10.1016/j.gloplacha.2009.07.007.
Hartmann, J., Moosdorf, N., Lauerwald, R., Hinderer, M., West, A.J., 2014a. Global chemical weathering and associated P-release — the role of lithology, temperature and soil properties. Chem. Geol. 363, 145–163. https://doi.org/10.1016/j.chemgeo.2013.10.025.
Hartmann, J., Lauerwald, R., Moosdorf, N., 2014b. A Brief Overview of the GLObal RIver Chemistry Database, GLORICH. Procedia Earth and Planetary Science 10, 23–27. https://doi.org/10.1016/j.proeps.2014.08.005.
Hijmans, R.J., 2019. Raster: Geographic Data Analysis and Modeling. R package version 2, 9–22. https://CRAN.R-project.org/package=raster.
Huscroft, J., Gleeson, T., Hartmann, J., Börker, J., 2018. Compiling and Mapping Global Permeability of the Unconsolidated and Consolidated Earth: GLobal HYdrogeology MaPS 2.0 (GLHYMPS 2.0). Geophys. Res. Lett. 45 (4), 1897–1904. https://doi.org/10.1002/2017GL075860.
Jansen, N., Hartmann, J., Lauerwald, R., Dürr, H.H., Kempe, S., Loos, S., Middelkoop, H., 2010. Dissolved silica mobilization in the conterminous USA. Chem. Geol. 270 (1–4), 90–109. https://doi.org/10.1016/j.chemgeo.2009.11.008.
Kaushal, S.S., Likens, G.E., Pace, M.L., Utz, R.M., Haq, S., Gorman, J., Grese, M., 2018. Freshwater salinization syndrome on a continental scale. Proc. Natl. Acad. Sci. U. S. A. 115 (4), E574–E583. https://doi.org/10.1073/pnas.1711234115.
Keller, C.K., 2019. Carbon exports from Terrestrial Ecosystems: a Critical-Zone Framework. Ecosystems 22 (8), 1691–1705. https://doi.org/10.1007/s10021-019-00375-9.
Lehmann, C.M.B., van Bowersox, C., Larson, S.M., 2005. Spatial and temporal trends of precipitation chemistry in the United States, 1985–2002. Environ. Pollut. 135 (3), 347–361. https://doi.org/10.1016/j.envpol.2004.11.016.
Likens, G.E., Driscoll, C.T., Buso, D.C., 1996. Long-Term Effects of Acid rain: Response and Recovery of a Forest Ecosystem. Science 272 (5259), 244–246. https://doi.org/10.1126/science.272.5259.244.
Livingstone, D.A., 1963. *Chemical composition of rivers and lakes* (Data of Geochemistry no. 440-G). Washington. pp. G1–G64. https://doi.org/10.3133/pp440G.
Ludwig, W., Amiotte Suchet, P., Munhoven, G., Probst, J.L., 1998. Atmospheric CO2 consumption by continental erosion: present-day controls and implications for the last glacial maximum. Global and Planetary Change 16-17, 107–120. https://doi.org/10.1016/S0921-8181(98)00016-2.
Ludwig, W., Amiotte Suchet, P., Probst, J.L., Hall, G.J., Meeson, B.W., Los, S.O., ... Landis, D.R., 2011. ISLSCP II Atmospheric Carbon Dioxide Consumption by Continental Erosion. https://doi.org/10.3334/ORNLDAAC/1019.
Mahowald, N., Ward, D.S., Kloster, S., Flanner, M.G., Heald, C.L., Heavens, N.G., ... Chuang, P.Y., 2011. Aerosol Impacts on Climate and Biogeochemistry. Annual Review of Environment and Resources 36 (1), 45–74. https://doi.org/10.1146/annurev-environ-042009-094507.
McClain, M.E., Boyer, E.W., Dent, C.L., Gergel, S.E., Grimm, N.B., Groffman, P.M., ... Pinay, G., 2003. Biogeochemical Hot Spots and Hot Moments at the Interface of Terrestrial and Aquatic Ecosystems. Ecosystems 6 (4), 301–312. https://doi.org/10.1007/s10021-003-0161-9.
Meybeck, M., 1979. Concentrations des eaux fluviales en éléments majeurs et apports en solution aux océans. Rev. Géol. Dynam. Géog. Phys. 21 (3), 215–246.
Meybeck, M., 1983. Atmospheric inputs and river transport of dissolved substances. Dissolved loads of rivers and surface water quantity/quality relationships 141, 173–192.
Meybeck, M., 1984. Les fleuves et le cycle géochimique des élements. Université de Paris, Paris.
Meybeck, M., 1986. Composition chimique des ruisseaux non pollués de France. Sciences Géologiques 39 (1), 3–77. https://doi.org/10.3406/sgeol.1986.1719.

Meybeck, M., 1987. Global chemical weathering of surficial rocks estimated from river dissolved loads. Am. J. Sci. 287, 401–428. https://doi.org/10.2475/ajs.287.5.401.

Meybeck, M., 2003. Global analysis of river systems: from Earth system controls to Anthropocene syndromes. *Philosophical Transactions of the Royal Society of London.* Series B, Biological Sciences 358 (1440), 1935–1955. https://doi.org/10.1098/rstb.2003.1379.

Moore, S.J., Bassett, R.L., Liu, B., Wolf, C.P., Doremus, D., 2008. Geochemical tracers to evaluate hydrogeologic controls on river salinization. Ground Water 46 (3), 489–501. https://doi.org/10.1111/j.1745-6584.2007.00420.x.

Moosdorf, N., Hartmann, J., Lauerwald, R., Hagedorn, B., Kempe, S., 2011. Atmospheric CO_2 consumption by chemical weathering in North America. Geochim. Cosmochim. Acta 75 (24), 7829–7854. https://doi.org/10.1016/j.gca.2011.10.007.

Moquet, J.-S., Guyot, J.-L., Crave, A., Viers, J., Filizola, N., Martinez, J.-M., ... Pombosa, R., 2016. Amazon River dissolved load: Temporal dynamics and annual budget from the Andes to the ocean. Environmental Science and Pollution Research International 23 (12), 11405–11429. https://doi.org/10.1007/s11356-015-5503-6.

Moré, J.J., 1978. The Levenberg-Marquardt algorithm: Implementation and theory. In: Watson, G.A. (Ed.), Lecture Notes in Mathematics. Numerical Analysis. 630. pp. 105–116. Berlin, Heidelberg: Springer Berlin Heidelberg. https://doi.org/10.1007/BFb0067700.

Oliva, P., Viers, J., Dupré, B., 2003. Chemical weathering in granitic environments. Chem. Geol. 202 (3–4), 225–256. https://doi.org/10.1016/j.chemgeo.2002.08.001.

Perri, F., Ietto, F., Le Pera, E., Apollaro, C., 2016. Weathering processes affecting granitoid profiles of Capo Vaticano (Calabria, southern Italy) based on petrographic, mineralogic and reaction path modelling approaches. Geol. J. 51 (3), 368–386. https://doi.org/10.1002/gj.2635.

Probst, J.L., 1992. Géochimie et hydrologie de l'érosion continentale. Mécanismes, bilan global actuel et fluctuations au cours des 500 derniers millions d'années Université Louis-Pasteur, Strasbourg Retrieved from. www.persee.fr/doc/sgeol_0302-2684_1992_mon_94_1.

Probst, J.L., Mortatti, J., Tardy, Y., 1994. Carbon river fluxes and weathering CO_2 consumption in the Congo and Amazon river basins. Appl. Geochem. 9, 1–13. https://doi.org/10.1016/0883-2927(94)90047-7.

Probst, J.L., Ludwig, W., Amiotte Suchet, P., 1997. Global modeling of CO_2 uptake by continental erosion and of carbon river transport to the oceans. / Modélisation à l'échelle globale des flux de CO_2 consommé par l'érosion continentale et des transports fluviaux de carbone vers les océans. *Sciences Géologiques*. Bulletin 50 (1), 131–156. https://doi.org/10.3406/sgeol.1997.1950.

R Core Team, 2018. R. Vienna, Austria: R Foundation for Statistical Computing. Retrieved from. https://www.R-project.org.

Raab, G., Egli, M., Norton, K., Dahms, D., Brandová, D., Christl, M., Scarciglia, F., 2019. Climate and relief-induced controls on the temporal variability of denudation rates in a granitic upland. Earth Surf. Process. Landf. 44 (13), 2570–2586. https://doi.org/10.1002/esp.4681.

Riebe, C.S., Hahm, W.J., Brantley, S.L., 2017. Controls on deep critical zone architecture: a historical review and four testable hypotheses. Earth Surf. Process. Landf. 42 (1), 128–156. https://doi.org/10.1002/esp.4052.

Roelandt, C., Goddéris, Y., Bonnet, M.P., Sondag, F., 2010. Coupled modeling of biospheric and chemical weathering processes at the continental scale. Glob. Biogeochem. Cycles 24 (2). https://doi.org/10.1029/2008GB003420.

Romero-Mujalli, G., Hartmann, J., Börker, J., Gaillardet, J., Calmels, D., 2019. Ecosystem controlled soil-rock pCO_2 and carbonate weathering – Constraints by temperature and soil water content. Chemical Geology. https://doi.org/10.1016/j.chemgeo.2018.01.030.

Schindler, D.W., 1988. Effects of Acid rain on Freshwater Ecosystems. Science 239 (4836), 149–157. https://doi.org/10.1126/science.239.4836.149.

Shangguan, W., Hengl, T., Mendes de Jesus, J., Yuan, H., Dai, Y., 2017. Mapping the global depth to bedrock for land surface modeling. Journal of Advances in Modeling Earth Systems 9 (1), 65–88. https://doi.org/10.1002/2016MS000686.

St Pierre, K.A., St Louis, V.L., Schiff, S.L., Lehnherr, I., Dainard, P.G., Gardner, A.S., ... Sharp, M.J., 2019. Proglacial freshwaters are significant and previously unrecognized sinks of atmospheric CO_2. Proceedings of the National Academy of Sciences of the United States of America 116 (36), 17690–17695. https://doi.org/10.1073/pnas.1904241116.

Stallard, R.F., Edmond, J.M., 1981. Geochemistry of the Amazon: 1. Precipitation chemistry and the marine contribution to the dissolved load at the time of peak discharge. J. Geophys. Res. 86 (10), 9844–9858.

Sun, X., Higgins, J., Turchyn, A.V., 2016. Diffusive cation fluxes in deep-sea sediments and insight into the global geochemical cycles of calcium, magnesium, sodium and potassium. Mar. Geol. 373, 64–77. https://doi.org/10.1016/j.margeo.2015.12.011.

Tipping, E., 1994. WHAMC—A chemical equilibrium model and computer code for waters, sediments, and soils incorporating a discrete site/electrostatic model of ion-binding by humic substances. Comput. Geosci. 20 (6), 973–1023. https://doi.org/10.1016/0098-3004(94)90038-8.

Velbel, M.A., 1993. Temperature dependence of silicate weathering in nature: how strong a negative feedback on term accumulation of atmospheric CO2 and global greenhouse warming? Geology 21, 1059–1062. https://doi.org/10.1130/0091-7613(1993)021%3C1059:TDOSWI%3E2.3.CO;2.

Vet, R., Artz, R.S., Carou, S., Shaw, M., Ro, C.-U., Aas, W., ... Reid, N.W., 2014. A global assessment of precipitation chemistry and deposition of sulfur, nitrogen, sea salt, base cations, organic acids, acidity and pH, and phosphorus. Atmospheric Environment 93, 3–100. https://doi.org/10.1016/j.atmosenv.2013.10.060.

Vörösmarty, C.J., McIntyre, P.B., Gessner, M.O., Dudgeon, D., Prusevich, A., Green, P., ... Davies, P.M., 2010. Global threats to human water security and river biodiversity. Nature 467 (7315), 555–561. https://doi.org/10.1038/nature09440.

Wadham, J.L., Tranter, M., Skidmore, M., Hodson, A.J., Priscu, J., Lyons, W.B., ... Jackson, M., 2010. Biogeochemical weathering under ice: Size matters. Global Biogeochemical Cycles 24. https://doi.org/10.1029/2009GB003688.

White, A.F., Blum, A.E., 1995. Effects of climate on chemical weathering in watersheds. Geochimica and Cosmochimica Acta 59 (9), 1729–1747. https://doi.org/10.1016/0016-7037(95)00078-E.

Wicke, B., Smeets, E., Dornburg, V., Vashev, B., Gaiser, T., Turkenburg, W., Faaij, A., 2011. The global technical and economic potential of bioenergy from salt-affected soils. Energy Environ. Sci. 4 (8), 2669. https://doi.org/10.1039/c1ee01029h.